You might find this additional info useful...

This article cites 74 articles, 27 of which can be accessed free at:
/content/111/1/197.full.html#ref-list-1

Updated information and services including high resolution figures, can be found at:
/content/111/1/197.full.html

Additional material and information about *Journal of Neurophysiology* can be found at:
http://www.the-aps.org/publications/jn

This information is current as of November 24, 2014.

An auditory colliculothalamocortical brain slice preparation in mouse

Daniel A. Llano,[1,2,3,4] **Bernard J. Slater,**[3] **Alexandria M. H. Lesicko,**[1] **and Kevin A. Stebbings**[3]

[1]*Department of Molecular and Integrative Physiology, University of Illinois at Urbana-Champaign, Urbana, Illinois;*
[2]*Beckman Institute, University of Illinois at Urbana-Champaign, Urbana, Illinois;* [3]*Neuroscience Program, University of Illinois at Urbana-Champaign, Urbana, Illinois; and* [4]*College of Medicine, University of Illinois at Urbana-Champaign, Urbana, Illinois*

Llano DA, Slater BJ, Lesicko AM, Stebbings KA. An auditory colliculothalamocortical brain slice preparation in mouse. *J Neurophysiol* 111: 197–207, 2014. First published October 9, 2013; doi:10.1152/jn.00605.2013.—Key questions about the thalamus are still unanswered in part because of the inability to stimulate its inputs while monitoring cortical output. To address this, we employed flavoprotein autofluorescence optical imaging to expedite the process of developing a brain slice in mouse with connectivity among the auditory midbrain, thalamus, thalamic reticular nucleus, and cortex. Optical, electrophysiological, anatomic, and pharmacological tools revealed ascending connectivity from midbrain to thalamus and thalamus to cortex as well as descending connectivity from cortex to thalamus and midbrain and from thalamus to midbrain. The slices were relatively thick (600–700 μm), but, based on typical measures of cell health (resting membrane potential, spike height, and input resistance) and use of 2,3,5-triphenyltetrazolium chloride staining, the slices were as viable as thinner slices. As expected, after electrical stimulation of the midbrain, the latency of synaptic responses gradually increased from thalamus to cortex, and spiking responses were seen in thalamic neurons. Therefore, for the first time, it will be possible to manipulate and record simultaneously the activity of most of the key brain structures that are synaptically connected to the thalamus. The details for the construction of such slices are described herein.

auditory; cortex; inferior colliculus; slice; thalamus

THE THALAMUS IS A CRITICAL checkpoint for all information that reaches the cerebral cortex. Despite many decades of investigation, its role in transforming information from the sensory periphery to the cortex remains largely unknown. A wide spectrum of hypothetical models of thalamic function have been proposed, ranging from those that postulate that the thalamus is a simple gated relay to those that propose that the thalamus plays a definite role in transforming the representation of information. Hybrid models exist that take into account the heterogeneity of thalamic nuclei, differences in the calcium-binding proteins expressed by thalamic neurons, and differences in the nature of descending control on thalamic function (Jones 2001; Sherman and Guillery 2011). One difficulty in fully testing these hypotheses is the absence of an experimental preparation that easily allows investigators to probe the inputs and the outputs of the thalamus simultaneously. Such a preparation would allow the investigator the opportunity to study systematically the synaptic mechanisms underlying the transformation of information that occurs at the level of the thalamus.

A partial solution is found in the thalamocortical slice preparation. In fact, key advances in our understanding of thalamocortical circuits have been made using brain slice preparations that retain connectivity between the thalamus and cortex. For example, Agmon and Connors (1991) developed a preparation containing connections between the ventral posterior nucleus and the barrel cortex, which has been instrumental in elucidating the synaptic mechanisms underlying the initial processing steps occurring as information from the thalamus reaches the barrel cortex (Gil et al. 1999; Lee et al. 2007; Llinas et al. 2002). In addition, this slice preparation has been important for the understanding of the synaptic physiology of the somatosensory corticothalamic projections (Castro-Alamancos and Calcagnotto 1999; Reichova and Sherman 2004) and corticothalamocortical projections (Theyel et al. 2010). Subsequent thalamocortical slice preparations from the auditory system (Cruikshank et al. 2002), visual system (MacLean et al. 2006), and anterior cingulate cortex (Lee et al. 2007) have also led to new insights regarding thalamocortical function, particularly in the auditory system (Hackett et al. 2011; Richardson et al. 2009; Verbny et al. 2006). A recently developed slice preparation containing retained projections from the auditory midbrain (inferior colliculus or IC) to the auditory thalamus (medial geniculate body or MGB) has been described (Lee and Sherman 2010). However, none of these slices retains projections from the sensory brain-stem inputs to the thalamus as well as outputs to the cortex, and studying these connections in a single-slice preparation will be critical for understanding the synaptic mechanisms underlying how the representation of information is transformed between peripheral structures and the cortex.

The goal of the current work was to develop a slice preparation that retains connectivity among the IC, MGB, and auditory cortex (AC). One limitation to the development of a new slice preparation is the rapid assessment of synaptic connectivity in any given slice. Traditionally, this is done either through neurophysiological means (e.g., field potentials or whole cell synaptic potentials) or tract tracing within the slice (e.g., biocytin or lipophilic dyes). Neither of these allows for rapid assessment (i.e., minutes) of the spatial distribution of connectivity in a slice, which is crucial for determining the degree of network connectivity within a new slice preparation. The use of flavoprotein autofluorescence imaging or NAD imaging, which measure the oxidation state of flavoproteins or NAD molecules, respectively, and therefore are indicators of neuronal activation, can rapidly facilitate assessment of slice connectivity. Flavoprotein autofluorescence is a highly sensitive marker of neuronal activation (Kosterin et al. 2005; Llano

Address for reprint requests and other correspondence: D. A. Llano, 2355 Beckman Institute, 405 N. Mathews, Urbana, IL 61801 (e-mail: d-llano@illinois.edu).

et al. 2009; Reinert et al. 2007; Shibuki et al. 2003), and since it is an intrinsic signal imaging technique, it does not involve the use of potentially toxic and heterogeneously loaded dyes. NAD imaging is also used in this study as an additional means to verify slice connectivity (Shuttleworth et al. 2003). Therefore, in the current study, we use optical as well as more traditional electrophysiological and anatomic means to develop and validate a slice preparation that preserves connectivity among the IC, MGB, and AC. This slice may therefore allow the dissection of the synaptic mechanisms underlying thalamic transformations of information en route to the cortex.

METHODS

Animals. Juvenile BALB/c mice, of both sexes, ages *postnatal day 12* (P12)–P21, and purchased from Harlan Laboratories, were used for these studies. Mice in the age ranges used in this study have been shown to have good hearing (Bartlett and Wang 2007), and it is known that mice, in general, rely on complex sounds for normal behavior (Holy and Guo 2005; Liu et al. 2003). Although there is significant brain growth across the ages of animals used in this study, no systematic attempt was made to alter the cutting procedure across these ages. All procedures were approved by the Institutional Animal Care and Use Committee at the University of Illinois. All animals were housed in animal care facilities approved by the American Association for Assessment and Accreditation of Laboratory Animal Care. Every attempt was made to minimize the number of animals used and to reduce suffering at all stages of the study.

After transcardiac perfusion and rapid removal of the brain, the brain was placed on wet filter paper, and an initial coronal cut was made to remove the anterior 2 mm of the forebrain (Fig. 1*A*). Similar to the work of Cruikshank et al. (2002), the brain was then tipped forward onto its cut side, and a 15° flap of tissue off of the right hemisphere was removed (Fig. 1*B*). Removal of this flap allows the

MGB and AC to be placed into the same cutting plane once the brain is flipped upside down (Fig. 1*C*). A key modification of the previous auditory thalamocortical slice preparation was to modify the cutting platform so that a 1.5-mm block of 2% agar was glued onto the platform. This block displaced the IC and hindbrain ventrally (i.e., upward, since the brain is upside down) so that the IC was in the same cutting plane as the MGB and AC (Fig. 1*D*). A vibratome was then used to obtain slices that contained IC, MGB, and AC (Fig. 1*E*). We initially cut slices at 700 μm but with experience have routinely been able to retain connectivity with 600-μm-thick slices. During experiments, the slices were placed on a wire mesh and elevated ~1 mm from the glass-bottom surface of the recording chamber (Fig. 1*F*). This allowed for artificial cerebrospinal fluid (ACSF) to flow above and below the slice, as described previously (Shibuki et al. 2003).

Auditory brain-stem responses. Animals were anesthetized with 100 mg/kg ketamine and 3 mg/kg xylazine before the insertion of two subdermal electrodes, one at the vertex and one behind the left ear. Stimuli were presented using a Tucker-Davis (TDT) System 3, EC1 closed-field speaker, with waveforms being generated by RPvdsEx software. An 8-kHz sinusoidal tone was presented for 5 ms (3 ms flat with 1 ms for both rise and fall times) at a rate of 2–6 Hz. Raw potentials were obtained with a Dagan 2400A amplifier and preamplifier headstage combination and filtered between 100 and 3,000 Hz. An ADInstruments PowerLab 4/30 box was used to average these waveforms 500–1,000 times. Visually apparent deflections within 10 ms after the onset of the stimulus were deemed a response. No effort was made to make statistical assessments of the deflections since the goal of these experiments was to show that the youngest animals assessed in this study simply had a functioning central auditory system.

Slice preparation. Mice were initially anesthetized with pentobarbital (25–50 mg/kg ip) and then transcardially perfused with an ice-cold sucrose saline solution (in mM: 206 sucrose, 10.0 MgCl$_2$, 11.0 glucose, 1.25 NaH$_2$PO$_4$, 26 NaHCO$_3$, 0.5 CaCl$_2$, 2.5 KCl, pH
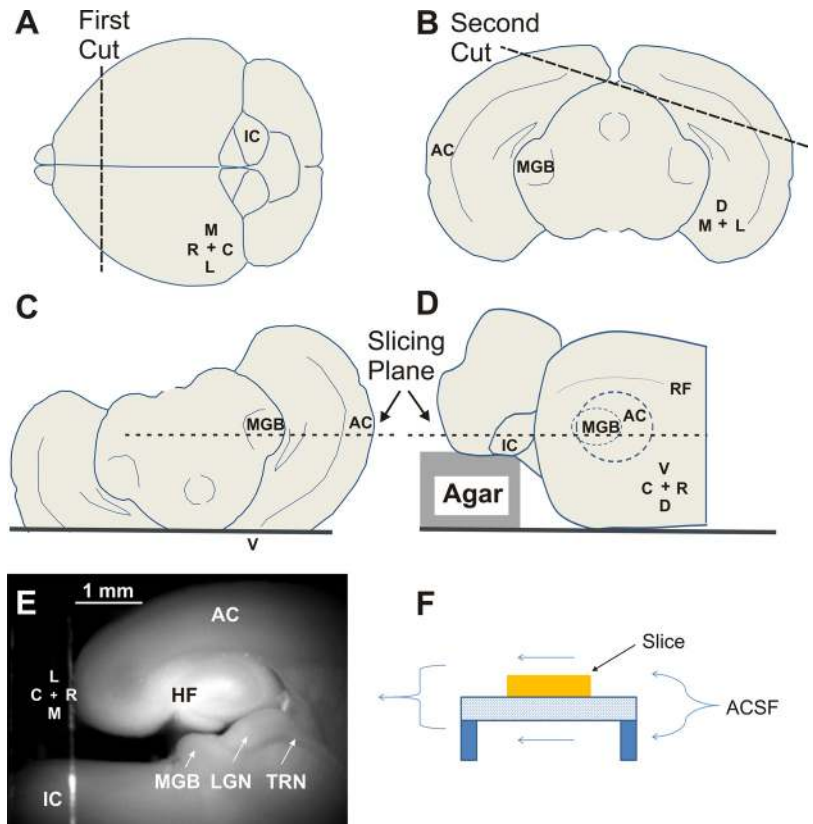

Fig. 1. Cutting procedure and establishing the viability of the auditory colliculothalamocortical slice in juvenile mice. *A*: an initial coronal cut is made to remove the olfactory bulbs and anterior 2 mm of the frontal cortex. *B*: a 15° slab is removed from the right cerebral cortex. *C* and *D*: the inferior colliculus (IC) is ventrally displaced by 1.5 mm to move it into the same cutting plane as the medial geniculate body (MGB) and auditory cortex (AC). *E*: a raw fluorescence photograph using a green fluorescent protein filter illustrating the relative locations of midbrain and thalamic and cortical structures in the connected slice. *F*: diagram illustrating double-sided perfusion of the slice. M, medial; C, caudal; L, lateral; R, rostral; D, dorsal; V, ventral; RF, rhinal fissure; HF, hippocampal formation; LGN, lateral geniculate nucleus; TRN, thalamic reticular nucleus; ACSF, artificial cerebrospinal fluid.

7.4) containing 1 mM kynurenic acid. Both the sucrose-saline solutions and kynurenic acid were used as neuroprotectants (Richerson and Messer 1995). Slices were then transferred to a holding chamber containing oxygenated incubation ACSF (in mM: 126 NaCl, 3.0 MgCl$_2$, 10.0 glucose, 1.25 NaH$_2$PO$_4$, 26 NaHCO$_3$, 1.0 CaCl$_2$, 2.5 KCl, pH 7.4) and incubated at 32°C for 1 h before experimentation.

Stimulation and imaging. Stimulation was generally done with glass micropipettes broken back to a diameter of 25–50 μm and filled with ACSF. We have also used carbon-fiber electrodes as well as bipolar tungsten electrodes with virtually identical results. Trains of electrical pulses were delivered using PowerLab software and hardware and a World Precision Instruments stimulus isolator. Unless otherwise indicated, trains were 1 s in duration, with 2-ms pulses, delivered at 40 pulses per second, and trains were delivered every 20 s, with 5 repetitions total. Focal application of glutamate or the AMPA-kainate blocker 6,7-dinitroquinoxaline-2,3-dione (DNQX; Tocris Bioscience) to the thalamus was achieved using a Toohey picospritzer. The picospritzer pipette was filled with 2 mM L-glutamate or 500 μM DNQX, was dissolved in ACSF, and had a diameter of 5 μm. Application pressure was 1–20 psi, with 2-ms pulse duration, 1-s pulse train, and pulse rate of 40 pulses per second. In some experiments, Alexa Fluor 594 (1.3 μM; A-10438; Invitrogen) was included in the pipette to assess the degree of diffusion of the injectate, which never extended beyond the MGB borders. Flavoprotein autofluorescence was done with a fluorescence illuminator (Prior Lumen 200) and a UMNIB Olympus filter cube (470- to 490-nm excitation, 505-nm dichroic, and 515-nm emission long pass). For NAD imaging (Shuttleworth et al. 2003), a Semrock Sirius-A-000 cube with 350- to 390-nm excitation and 415- to 465-nm emission was used. A coverslip was placed over the slice to provide a stable imaging plane. Unless otherwise indicated, data were collected using an infinity-corrected ×2 macroobjective (0.13 numerical aperture) and a Retiga EXi camera using 4 × 4 binning and StreamPix software.

Analysis of imaging data. Most imaging movies were obtained at 4 frames per second and acquired for ~105 s, generating movies of ~420 images. Because of the known reversible quenching of the flavoprotein signal (Husson and Issa 2009; Kubota et al. 2008), the time series of each pixel was either low-pass filtered or had a polynomial-fit curve subtracted from the raw traces. To display time series analyses (see below), a 3-pixel spatial smoothing kernel was used. Time-domain and frequency-domain analyses were performed on imaging data. Most data were analyzed using time-domain techniques. For this, the 1st 20 frames (5 s) of prestimulus data were used as a baseline, and the responses were expressed as a change in fluorescence over baseline fluorescence (Δf/f × 100%). For frequency-domain analysis, a discrete Fourier transform was performed on each time series, and the spectral power at the stimulation frequency (usually 0.05 Hz) was extracted. As we previously did (Llano et al. 2009), we have provided arbitrary units for the Fourier maps since the signal strength at any given pixel is dependent on strength of illumination and tissue illumination and image acquisition time, which were optimized for each experiment, thus making values of signal power at any given frequency arbitrary. The use of arbitrary units in Fourier analysis, like all techniques used to produce images normalized to peak amplitude, has the potential to produce noisy images when signal amplitude is low. In practice, however, since spectral power is often strong at either the stimulus or the response site, we rarely encountered this problem.

Patch-clamp recording. Whole cell recordings were performed using a visualized slice setup outfitted with infrared-differential interference contrast (IR-DIC) optics and performed at 30–32°C. Recording pipettes were pulled from borosilicate glass capillary tubes and had tip resistances of 2–5 MΩ when filled with recording solution [in mM: 117 K-gluconate, 13 KCl, 1.0 MgCl$_2$, 0.07 CaCl$_2$, 0.1 EGTA, 10.0 HEPES, 2.0 Na-ATP, 0.4 Na-GTP, and 0.5% biocytin, pH 7.3]. For cell-attached recordings, all procedures were identical, but the membrane seal was not broken. A MultiClamp 700B amplifier (Molecular Devices, Sunnyvale, CA) and pCLAMP software (Molecular Devices) for data acquisition (20-kHz sampling) were used.

Tract tracing and immunostaining. Biocytin and 1,1′-dioctadecyl-3,3,3′,3′-tetramethylindocarbocyanine perchlorate (DiI) were used for tract tracing. For biocytin (Sigma), a dry crystal was carefully placed on the IC of the slice while in the slice chamber. The slice remained in the chamber for several hours before being placed in an incubation chamber with oxygenated ACSF and bubbled overnight. The slice was then fixed in 4% paraformaldehyde (PFA) in PBS. After graded saturation in 30% sucrose, the slices were resectioned at 75 μm and processed for cobalt-intensified diaminobenzidine. For DiI (D-282; Invitrogen) tracing, DiI crystals were carefully placed on sections that were fixed for 1–2 h in 1% PFA and then allowed to incubate in a dark, humidified chamber for 1–5 days. Sections were then fixed in 4% PFA in PBS, whole-mounted, and photographed using a traditional fluorescence microscope for low-power images (Olympus IX71) and a laser-scanning confocal microscope (Leica SP2 Visible Laser Confocal Microscope) for high-power images.

For parvalbumin immunostaining, slices prepared as described above were fixed in 4% PFA and resectioned at 75 μm. To enhance membrane permeability, sections were incubated for 30 min in a solution of 0.3% Triton X-100 in PBS. The sections were then transferred to a blocking solution consisting of 0.3% Triton X-100 and 3% goat serum in PBS and incubated for 30 min. Primary antibody solution consisted of 1:500 anti-parvalbumin monoclonal antibody (P3088; Sigma) in the blocking solution. Sections were incubated in primary antibody solution overnight and rinsed in three changes of the Triton X-100 solution the following day. Afterward, the sections were transferred to a secondary antibody solution consisting of 1:100 Alexa Fluor 488-nm secondary antibody (A11001; Molecular Probes) and incubated at room temperature for 2 h. Following a final series of washes in PBS, the sections were mounted on gelatin-coated slides and coverslipped with an anti-fade solution (VECTASHIELD; Vector Laboratories).

2,3,5-Triphenyltetrazolium chloride (TTC) was used to assess tissue health. A solution consisting of 2% TTC (T-8877; Sigma) in standard ACSF was prepared fresh for each experiment and protected from exposure to light. Each slice was placed in an individual well of a culture plate and completely immersed in the staining solution. The slices were incubated in the dark at 37°C for 30 min. To ensure an even reaction, slices were elevated on a wire net and flipped halfway through the incubation period. Slices were then rinsed in three changes of 0.1 M PBS, pH 7.4, and fixed overnight in 4% PFA. Following fixation, slices were cryoprotected in an ascending gradient of sucrose up to 30% in PBS. Slices were cut cross-sectionally (90° to the original cutting plane) to best observe variations in TTC staining with slice thickness. To analyze the pattern of TTC staining, images were imported into ImageJ (http://rsbweb.nih.gov/ij) and had lookup tables inverted, and a ratio was computed of the staining density at the center of the slice to the peak staining density just deep to the surface. A ratio of 1.0 corresponds to no measurable change in cell viability toward the inner portions of the slice, whereas lower ratios correspond to decreases in cell viability toward the inner portions.

Statistical analysis. Given the relatively small numbers of slices or cells being compared in this study, Gaussian distributions were not assumed, and nonparametric tests were therefore used. All statistical analyses were done in GraphPad software (La Jolla, CA).

RESULTS

Auditory brain-stem responses and slice viability. Auditory brain-stem responses (ABRs) were obtained from juvenile mice to establish that mice at ages from which brain slices were obtained have a functioning auditory system. Similar to ABRs in older animals, ABRs were observed in animals as young as P12 and qualitatively demonstrate at least 4 positive-going
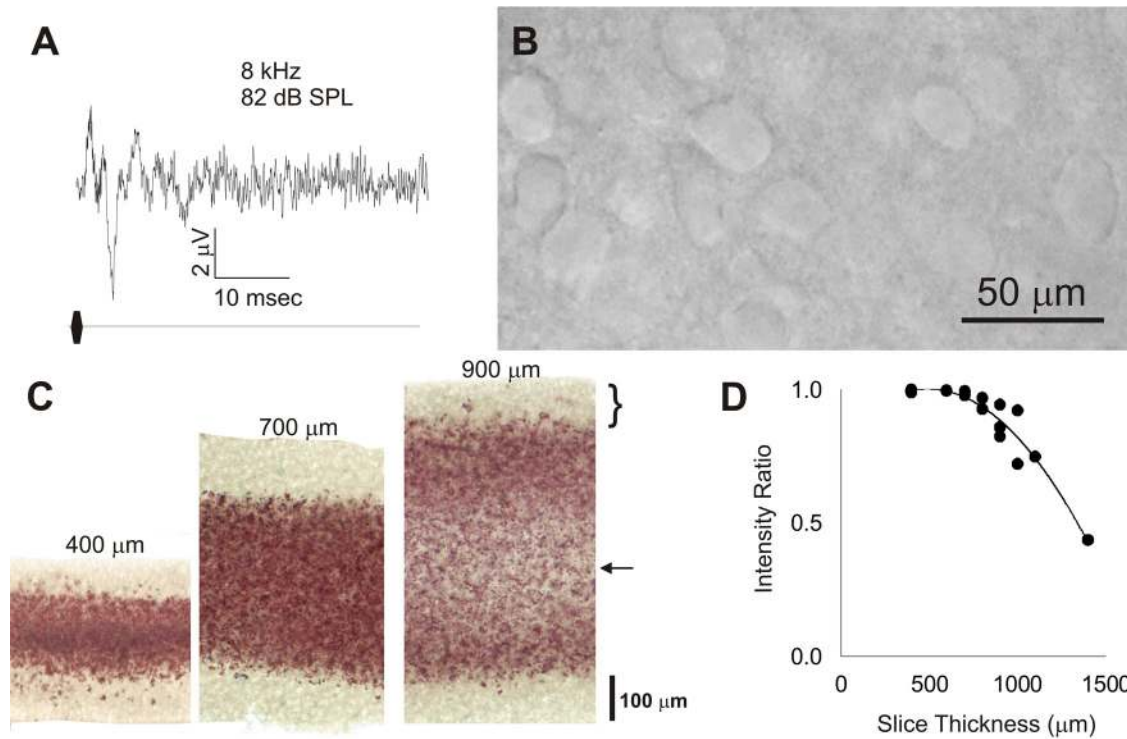
Fig. 2. *A*: auditory brain-stem response taken from a mouse pup at *postnatal day 12*, taken as an average of 1,000 trials. SPL, sound-pressure level. *B*: differential interference contrast image from the cerebral cortex of a 600-μm thick slice ~4 h after slicing. *C*: 2,3,5-triphenyltetrazolium chloride (TTC)-stained slices obtained from slices cut at 400, 700, and 900 μm. Bracket corresponds to pale area on the perimeter of all of the slices corresponding to poor TTC signal. Arrow corresponds to the pale area in the interior of the 900-μm slice, suggesting poor viability in this portion of the thick slice. *D*: plot of the ratio of TTC staining intensity in the center of the slice vs. peak intensity just deep to the surface vs. thickness. Data were pooled from 6 different animals. Equation for fit curve: $y = -7\text{E}-07x^2 + 0.0007x + 0.8364$, $r^2 = 0.92$.

peaks over the 1st 10 ms after click onset (Fig. 2*A*). Animals at younger or older ages were not assessed.

To assess the viability of colliculothalamocortical slices, slices up to 700 μm thick were examined 3–4 h after cutting. The appearance of the cerebral cortical or midbrain tissue under DIC optics revealed many normal-appearing neurons (Fig. 2*B*), which were found to have normal physiological parameters. The data for all cells recorded from 600- and 700-μm thick slices, in both connected and unconnected slices, are shown in Table 1. The mean resting membrane potentials were more negative than −60 mV and did not differ across regions [IC: −60.6 ± 5.5 (SD) mV, MGB: −60.9 ± 7.1 mV, AC: −64.0 ± 11.4 mV; $P = 0.12$, Kruskal-Wallis nonparametric ANOVA]. The mean spike heights were >50 mV in all regions but tended to be smallest in the MGB [IC: 59.7 ± 11.8 (SD) mV, MGB: 51.8 ± 6.4 mV, AC: 62.9 ± 10.6 mV; $P = 0.001$, Kruskal-Wallis nonparametric ANOVA]. The mean input resistance was >150 MΩ in all regions and was largest

in the IC [IC: 389 ± 233 (SD) MΩ, MGB: 202 ± 37 MΩ, AC: 152 ± 73 MΩ; $P = 0.001$, Kruskal-Wallis nonparametric ANOVA].

Assessment of TTC-stained slices revealed that slices cut at 400 μm, which is generally considered to be well within the viability range for slice studies, demonstrated poorly stained pale areas on the perimeter of the tissue, comprising the outer 50–100 μm, indicating an absence of mitochondrial-reducing enzymes that are typically found in viable tissue. The interior of the slice, however, stained a deep red color, suggesting intact mitochondrial systems and good tissue viability (Fig. 2*C, left*). As slice thickness increased, this same pattern was replicated at 700 μm. At 900 μm in thickness, the innermost portion of the slices remained poorly stained, suggesting lower tissue viability in this region (Fig. 2*C, right*). A similar pattern was seen across slices from 6 different animals. The ratio of the TTC staining intensity in the center of the slice to the peak TTC staining intensity just deep to the surface was plotted across 20 different data points from 6 different animals and is shown in Fig. 2*D*. The ratio remains near 1.0 up to ~800 μm and then drops off at greater depths. For this reason, all data demonstrated herein are restricted to slices 700 μm or less in thickness.

Ascending pathway. Electrical stimulation of the central nucleus of the inferior colliculus (ICc) led to activation of the external cortex of the inferior colliculus (ECIC), MGB, and AC. A small portion of the thalamic reticular nucleus (TRN) was often observed to be activated as well (Fig. 3*A*). Two more representative slices from different animals are shown in Fig.

Table 1. *Cell parameters recorded in 600- and 700-μm-thick slices*

	IC, n = 12	MGB, n = 46	AC, n = 42
Resting potential, mV	−60.6 ± 5.5	−60.9 ± 7.1	−64.0 ± 11.4
Spike height, mV*	59.7 ± 11.8	51.8 ± 6.4	62.9 ± 10.6
Input resistance, MΩ*	389 ± 233	202 ± 37	152.6 ± 73

Values are means ± SD. *$P < 0.001$, Kruskal-Wallis nonparametric ANOVA. IC, inferior colliculus; MGB, medial geniculate body; AC, auditory cortex.
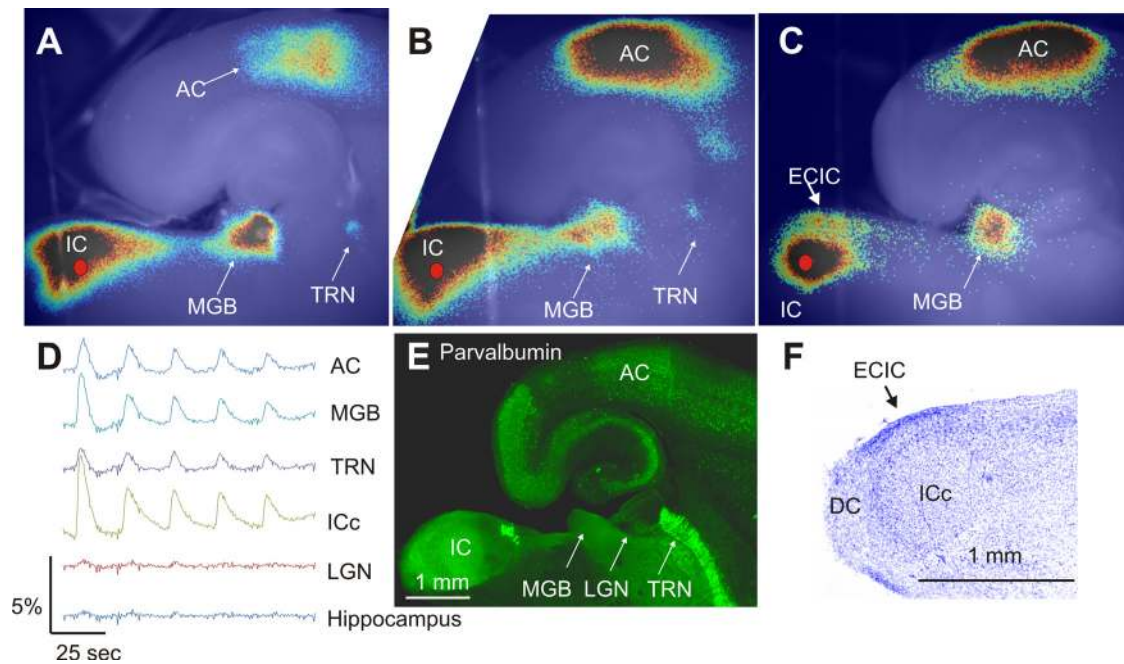
Fig. 3. Establishing the connectivity and structures within the slice. *A*: Fourier image demonstrating that electrical stimulation of the inferior colliculus (ICc; red filled circle) produces activation of the MGB, TRN, and AC. *B* and *C*: 2 additional slices from other animals demonstrating representative activations. *D*: time course of activation in 5 different regions of interest taken from the slice shown in *A*. Each region of interest = a square of 10×10 pixels or approximately 280×280 μm. *E*: parvalbumin-immunostained section demonstrating high density of parvalbumin in the AC, IC, MGB, as well as the entorhinal cortex. *F*: Nissl-stained section demonstrating the presence of the ICc, external cortex of the inferior colliculus (ECIC), and dorsal cortex (DC).

3, *B* and *C*. As shown, not all slices displayed clear TRN activation (Fig. 3*C*), but all showed strong MGB and AC activation. Flavoprotein activation was limited to known targets of auditory structures such that little flavoprotein activation signal was seen in neighboring structures, such as the lateral geniculate nucleus or hippocampus (Fig. 3*D*, taken from the slice shown in Fig. 3*A*). As demonstrated in Fig. 3*D*, within a single run using repeated stimulation, the amplitude of the flavoprotein response showed habituation within an individual run, although this habituation did recover between runs.

Immunostaining of slices that were resectioned at 75 μm and reacted with an anti-parvalbumin antibody demonstrated high parvalbumin signal in the areas of thalamus and cortex activated after electrical stimulation of the ICc (Fig. 3*C*). Nissl staining of the slice preparation revealed three distinct regions within the IC, similar to previous studies (Beyerl 1978; Faye-Lund and Osen 1985; Meininger et al. 1986). At the most dorsocaudal pole of the slice, a region of large, loosely packed cells was observed, likely representing the dorsal cortex (DC). A thin band of more densely packed cells was observed at the

lateral border, likely representing the ECIC, and a large central region was observed with relatively small and densely packed cells, likely representing the ICc (Fig. 3*D*). This pattern was replicated in three out of three slices processed in this manner.

To assess whether AC activation after IC stimulation was caused by antidromic activation of corticocollicular afferents or disynaptic orthodromic activation of MGB followed by activation of the AC, AMPA and kainate receptors in the MGB were blocked by focal application of DNQX to the MGB just before IC stimulation. In three out of three slices, we found that focal application of 500 μM DNQX to the MGB reversibly and strongly diminished IC stimulation-induced activation of the MGB, TRN, and AC (see Fig. 4, *A–C*, for an example).

An additional form of metabolic imaging, NAD imaging, was also used to verify connectivity within the slice. NAD imaging demonstrates similar pattern of activation across IC, MGB, and AC as flavoprotein imaging (Fig. 5), although the waveforms for NAD are negative-going rather than positive-going in the case of flavoprotein imaging (Fig. 5*A*, *inset*). In all five slices examined with both flavoprotein and NAD imaging,
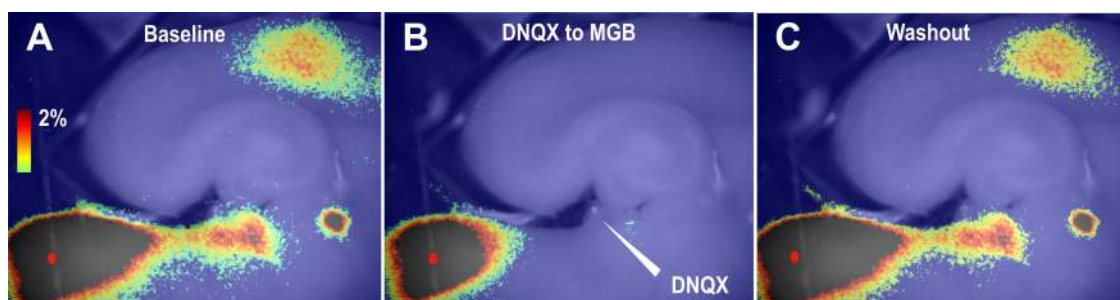

Fig. 4. Same slice as in Fig. 3, using change in fluorescence ($\Delta f/f$) images, showing the pattern of activation seen before 6,7-dinitroquinoxaline-2,3-dione (DNQX) application to the MGB (*A*), during DNQX application (*B*), and after washout (*C*).
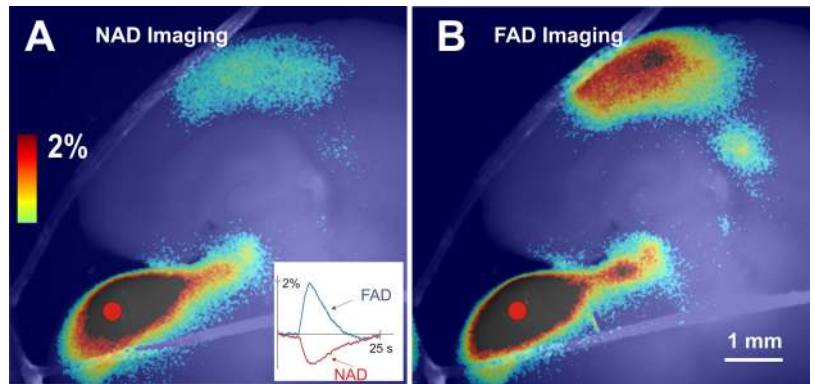
Fig. 5. NAD vs. flavoprotein (FAD) imaging. *A*: Δf/f image of colliculothalamocortical activation after stimulation in the IC (red circle), imaged using NAD imaging. *Inset* shows time course of AC activation in the same slice using flavoprotein imaging in blue and NAD imaging in red. *B*: Δf/f image of same slice, imaged using flavoprotein imaging.

both forms of imaging produced very similar patterns of activation, although the NAD signal was always slightly smaller than the flavoprotein signals [mean peak of flavoprotein activation = 1.7 ± 0.18 (SE)% vs. mean absolute value peak of NAD activation = −0.9 ± 0.14 (SE)%; $P = 0.008$, Mann-Whitney rank-sum test].

Electrical stimulation of the IC drives synaptic potentials in both the MGB and AC. In the MGB, 11 cells were recorded in whole cell mode that received synaptic input from IC. A range of synaptic input patterns were observed in the MGB after IC stimulation, including pure excitatory postsynaptic potentials (EPSPs; 3 out of 11 cells), pure inhibitory postsynaptic potentials (IPSPs; 6 out of 11 cells), and mixtures of both (2 out of 11 cells; Fig. 6, *A–C*). Cell-attached recordings revealed a small number of neurons in the MGB that fired action potentials in response to IC stimulation (see Fig. 6*D* for poststimulus time histogram). IC stimulation also produced EPSPs in the AC, but no IPSPs were seen, and no spiking responses were observed ($n = 6$; Fig. 6*E*). The mean latency PSPs in the MGB were shorter than in the AC [5.7 ± 0.9 (SE) ms, $n = 11$ vs. 12.8 ± 1.5 (SE) ms, $n = 6$; $P = 0.004$, Mann-Whitney rank-sum test; Fig. 6*F*].

Descending projections. Portions of the descending pathways also appeared to be retained in this slice preparation. Electrical stimulation of the AC often produced activation of several subcortical structures, such as a small region of the corpus striatum, MGB, and IC (Fig. 7*A*). Our success rate of retaining descending connections within the slice was substantially lower than with the ascending connections (approxi-

mately 25 vs. 75%). Since the mouse corticocollicular pathway appears to descend, in part, through the most ventral portions of the thalamus (http://connectivity.brain-map.org/projection/experiment/157954927), we explored alterations of the slice to increase the steepness of the angle between the AC and MGB (to 45°) as well as to displace more ventrally the IC (up to 2.5 mm) to align it with the most ventral portions of the MGB. This only marginally increased our success rate, and these data are not shown.

Placement of several crystals of DiI into the AC after light fixation of the slice led to labeling of long-range afferents to the MGB and to the IC, with terminations present in the MGB, ECIC, and DC (Fig. 7, *B–D*).

Whole cell recording in the ECIC after stimulation in the AC demonstrated long-range responses in a neuron with a pause-regular spiking profile with primary dendrites extending medially, rostrally, and laterally from the cell body (Fig. 8*A*). After electrical stimulation with 500 μA in the AC, EPSPs were relatively large [average 4.4 ± 0.95 (SD) mV], blocked with bath-applied DNQX, and returned with washout of DNQX (Fig. 8*C*). EPSPs were seen with electrical stimulation amplitudes as low as 25 μA (data not shown). Repetitive stimulation at 10 pulses per second diminished EPSP amplitude by ~40% (Fig. 8*D*). We recorded from 6 IC cells with synaptic input from cortical afferents. These cells had a mean latency of 7.4 ± 2.3 (SD) ms, and all showed EPSPs.

The thalamocollicular system was also investigated. Electrical stimulation was not used in the thalamus for these experiments because of the potential to activate corticocollicular
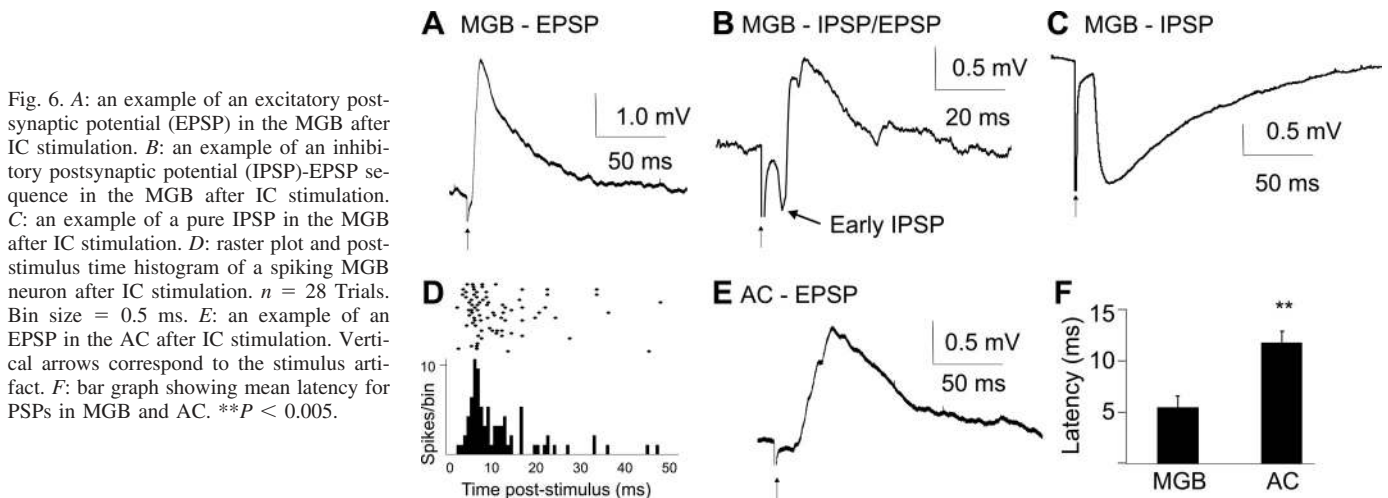
Fig. 6. *A*: an example of an excitatory postsynaptic potential (EPSP) in the MGB after IC stimulation. *B*: an example of an inhibitory postsynaptic potential (IPSP)-EPSP sequence in the MGB after IC stimulation. *C*: an example of a pure IPSP in the MGB after IC stimulation. *D*: raster plot and poststimulus time histogram of a spiking MGB neuron after IC stimulation. $n = 28$ Trials. Bin size = 0.5 ms. *E*: an example of an EPSP in the AC after IC stimulation. Vertical arrows correspond to the stimulus artifact. *F*: bar graph showing mean latency for PSPs in MGB and AC. ** $P < 0.005$.
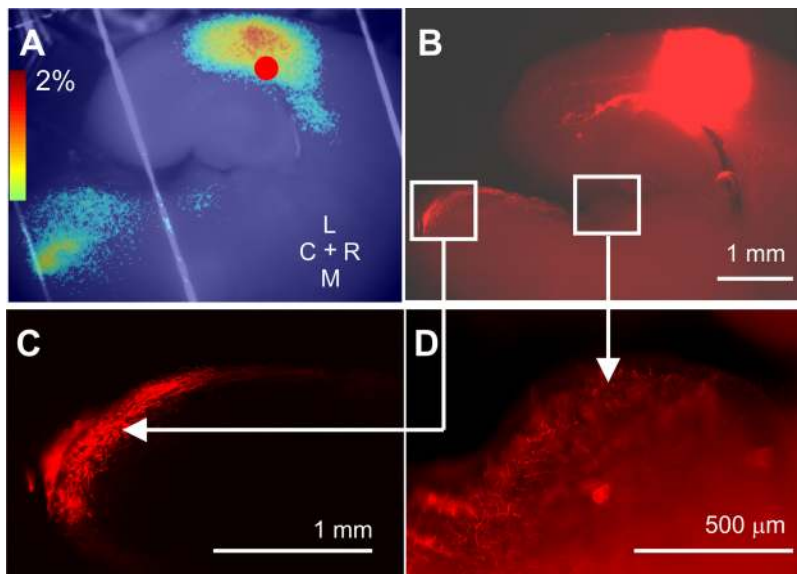
Fig. 7. Descending connectivity within the slice. *A*: Δf/f map of the result of electrical stimulation of the AC with subsequent activation of MGB and IC. *B*: low-magnification (×2) view of 1,1′-dioctadecyl-3,3,3′,3′-tetramethylindocarbocyanine perchlorate (DiI) application to the AC showing label in the ECIC and DC. *C*: high-magnification (×20) view of confocal image of square region shown in *B* demonstrating synaptic terminals in the ECIC and DC. *D*: high-magnification (×40) image of labeled terminals in the MGB in the same slice.

fibers of passage. Therefore, picospritzer-based application of 2 mM glutamate was used in the caudal-medial portion of the MGB, which is known to contain thalamocollicular neurons (Kuwabara 2012; Kuwabara and Zook 2000; Senatorov and Hu 2002; Winer et al. 2002). A small focus of activation was seen at the ECIC-DC border (Fig. 9*A*). Placement of a crystal of biocytin into this area of the IC produced substantial anterograde label in the MGB as well as a small amount of retrogradely labeled thalamocollicular cell bodies in the caudal-medial portions of the MGB, seen at low (Fig. 9*B*) and high power (Fig. 9*C*).

DISCUSSION

In the current study, we describe a new method for the generation of viable brain slices for the simultaneous stimula-
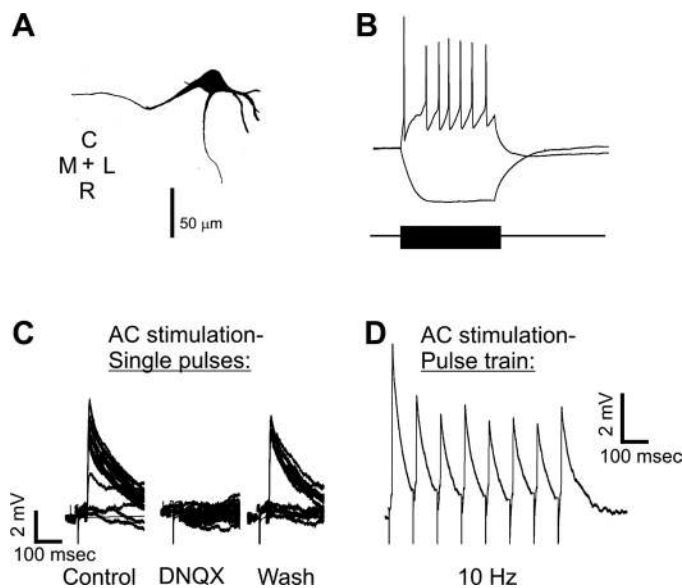

Fig. 8. *A*: morphological reconstruction of a cell in the ECIC that was responsive to AC stimulation. *B* and *C*: whole cell patch response to inward and outward current injection (*B*) and synaptic responses of this cell to electrical stimulation of the AC under control conditions under bath-applied DNQX and after wash (*C*). *D*: response of same cell to electrical stimulation of AC at 10 Hz demonstrating habituating responses.

tion and measurement of activity of the mouse IC, MGB, TRN, and AC. Slice connectivity was confirmed using flavoprotein autofluorescence imaging, NAD imaging, whole cell recordings along several brain structures, and tract tracing. This slice has retained projections from the IC to the MGB and from the MGB to the AC as well as connectivity between the TRN and MGB. Long descending pathways are preserved with lower yield, and these include both the corticocollicular pathway and the thalamocollicular pathway. Nissl staining of the slices suggested that the three major divisions of the IC (DC, ECIC, and ICc) are present in this slice (Beyerl 1978; Faye-Lund and Osen 1985; Meininger et al. 1986). In addition, given the retention of parvalbumin immunostaining in activated regions of the MGB and AC, it is likely that the slice contains at least substantial proportions of the ventral division of the MGB and the primary AC (Budinger et al. 2000; Cruikshank et al. 2001; Hashikawa et al. 1991; Llano and Sherman 2008; Wallace et al. 1991). However, given the thickness of the slice, we cannot exclude that at least a portion of the depth of the slices contain portions of the dorsal division of the MGB.

Methodological considerations. To achieve a high degree of connectivity, thick slices (600–700 μm) were obtained, which raises the possibility that the portions of the slices had poor viability. Several manipulations were done to maximize slice health such as transcardiac perfusion before removal of the brain, use of kynurenic acid in a sucrose saline solution for perfusion and cutting (Richerson and Messer 1995), and elevation of the slice to allow double perfusion (Shibuki et al. 2003). Usual parameters, such as the appearance of the tissue under DIC optics, resting membrane potentials, spike amplitudes, and synaptic potentials, all appeared normal. In addition, TTC staining, which is a sensitive marker for neuronal parenchymal health (Aitken et al. 1995; Hatfield et al. 1991; Mathews et al. 2000), did not indicate a lack of tissue health up to 700 μm but did find less viable tissue in the interior regions of the slice at 900 μm. Although it is possible that the innermost regions of the 900-μm slices did not take up TTC because of poor diffusion, this would not diminish the main finding that the 700-μm slices showed good uptake throughout the inner regions. It is likely that the TTC staining would have
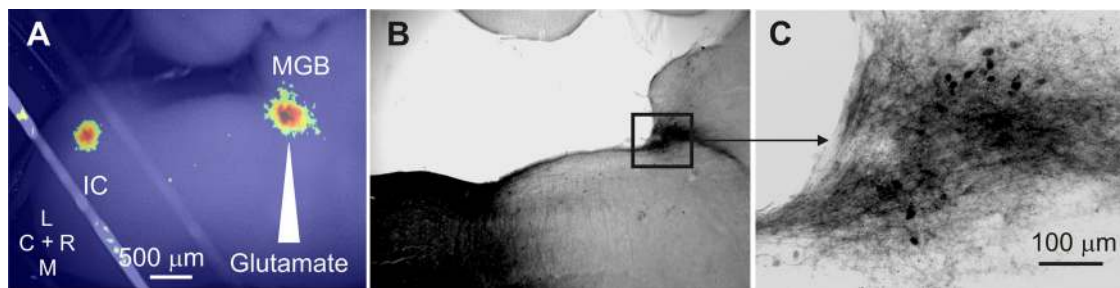
Fig. 9. *A*: Fourier image demonstrating that picospritzer application of 2 mM glutamate to caudodorsal part of MGB activates a small region of the ECIC. *B* and *C*: deposition of biocytin into the slice in the IC showing retrograde label in caudodorsal MGB at 4 and ×20 magnification.

uncovered unhealthy tissue in the interior of the slice if it was there because the TTC staining did reveal poorly viable tissue at the tissue margins. This poor staining at the tissue edges correlates to the well-known anecdotal evidence among slice physiologists that the most superficial regions of brain slices do not contain viable cells, likely because of slicing trauma. Other potential manifestations of hypoxia, such as epileptiform activity, which is easily observed using flavoprotein autofluorescence, were never observed in our experiments. Finally, it is also worth mentioning that several other investigators have successfully used 600-μm slices for their experiments (Cruikshank et al. 2002; Smith et al. 1991; Spergel et al. 2001). Therefore, it is likely that the slices used in the current study are viable for physiological studies.

Another potential methodological concern is the use of flavoprotein autofluorescence and NAD imaging as a tool to investigate the slice. These methods were used because of their ease of use and their ability to allow rapid assessment of the connectivity of any given slice. In addition, the NAD imaging, by using shorter wavelengths for excitation and emission than flavoprotein imaging, may offer flexibility to the experimenter if these imaging techniques are to be combined with other optical techniques. However, activation of flavoprotein and NAD signals are relatively slow, peaking at 1–2 s and returning to baseline at ~15 s (Husson et al. 2007; Llano et al. 2009; Reinert et al. 2007; Shibuki et al. 2003; Shuttleworth et al. 2003), and, as shown here, the NAD signal is slightly weaker than the flavoprotein signal (Fig. 5). Given the slow time courses of these signals, flavoprotein and NAD imaging are likely not suitable to capture the order of activation or to separate direct vs. recurrent activation of any of the structures in the slice. However, it is worth noting that any other method of assessment that may have better temporal resolution, such as voltage-sensitive dye imaging, calcium imaging with single- or two-photon microscopy, or electrical recordings, are fully compatible with the use of this connected slice preparation.

Most of the stimulation used in the current study was electrical rather than done with techniques that primarily activate neurons orthodromically (e.g., glutamate-based stimulation techniques). This raises the possibility that the activations seen, at least in part, were driven by antidromic activation. Electrical stimulation was used to drive polysynaptic responses (i.e., from IC to MGB and then to drive MGB to AC). In our experience, and in the experience of others (Katz and Dalva 1994; Llano and Sherman 2009; Shepherd et al. 2003), glutamate-based methods of stimulation are very unlikely to produce enough synaptic drive to produce polysynaptic responses that would allow the observation of AC activation after IC

stimulation. Therefore, the polysynaptic responses elicited by electrical stimulation revealed a broader network of relevant structures than would have been apparent if glutamate-based stimulation had been used in the IC. For example, it is likely that the activation in the central nucleus of the IC seen in Fig. 7*A* is polysynaptic since it is known that the majority (if not all) of the projections from the AC to the IC are to the external and dorsal cortices of the IC (Bajo et al. 2007; Malmierca and Ryugo 2011; Saldaña et al. 1996). This is consistent with our DiI tracer analysis (Fig. 7, *B–D*), where all of the corticocollicular terminals were seen in the external and dorsal cortices. In the current study, focal blockade of AMPA/kainate receptors with application of DNQX to the MGB or global blockade with bath application of DNQX eliminated IC-MGB-AC transmission (Fig. 4) and corticocollicular transmission (Fig. 8), respectively. In addition, the latency analysis (Fig. 6*F*) suggests sequential activation of MGB followed by AC, and the relatively long latencies seen in the IC (average 7.4 ms) are also consistent with orthodromic activation. It should be noted that the latencies seen in this study are somewhat longer than latencies seen in other slice studies (Agmon and Connors 1992; Finlayson and Cynader 1995) but similar to some others (Kawaguchi et al. 1989; Li et al. 1999; Miles and Wong 1987). The long latencies may reflect the long distances involved in the current study compared with other studies, the relatively low temperatures used (30–32°C), and/or potentially polysynaptic activation that may be more likely in this study given the size and thickness of the slices used.

Potential uses of this slice preparation. Given the relatively poor understanding of the role of the thalamus in modifying sensory information, this novel slice preparation has the potential to permit a detailed investigation of the influences of multiple elements, such as the TRN, other thalamic regions, and focal pharmacological manipulations, on IC-MGB-AC transmission. For example, the responses of various brain structures in response to temporally patterned stimuli indicate that a significant transformation in the representation of these sounds occurs as signals ascend through the central auditory pathways (Langner 1992). Specifically, along the midbrain-thalamus-cortical pathway, there is a dramatic reduction in the ability of individual neurons to time-lock their responses to patterned stimuli, but many of these neurons show maximum responses at particular rates of stimulation (Bartlett and Wang 2007; Llano and Feng 1999; Ter-Mikaelian et al. 2007). These data suggest that this slice preparation may be useful to study the detailed synaptic mechanisms underlying this transformation for excitatory and inhibitory integration in the MGB.

Another potential use of this slice is to study the interaction between top-down (e.g., corticothalamic) and bottom-up (e.g., colliculothalamic) signals at the level of the thalamus. This type of experiment has been done in preparations without retained connections to AC and IC by using electrical stimulation of cut corticothalamic and colliculothalamic axons (Smith et al. 2007). However, without full connectivity to IC and AC, this approach is limited because of the potential for antidromic stimulation of thalamocortical or thalamocollicular fibers and because of the inability to measure simultaneous activation in the AC. In addition, we, as others have (Bartlett and Smith 1999; Peruzzi et al. 1997), found a variety of excitatory and inhibitory patterns of synaptic input to the MGB from the IC (Fig. 6). How such ascending inhibitory inputs may interact with GABAergic inputs from the TRN and/or excitatory input from AC is not yet known and could potentially be investigated further with this preparation. Finally, descending projections to the IC may be studied with the slice, although the yield of producing intact slices is lower for the corticocollicular pathway. The corticocollicular pathway may be of substantial importance for sound processing. For example, it is known that this pathway can substantially modify the response of neurons in the IC and that there is substantial heterogeneity in this pathway in terms of underlying physiological properties and effects on IC neurons (Bajo and Moore 2005; Bajo et al. 2010; Jen et al. 2001; Mitani et al. 1983; Schofield 2009; Slater et al. 2013; Suga and Ma 2003; Yan and Ehret 2002; Yan et al. 2005). Finally, a little-described but evolutionarily ancient pathway exists from the posterior thalamus to the IC (Feng and Lin 2004; Kuwabara 2012; Kuwabara and Zook 2000; Senatorov and Hu 2002; Winer et al. 2002) and, when stimulated, appears to activate the external cortex of the IC focally (Fig. 9A). This is consistent with previous work by Kuwabara and Zook (2000) demonstrating that thalamotectal fibers primarily target the nonprimary portions of the IC. The synaptic physiology of both of these pathways can be investigated using this slice preparation.

Limitations of this slice preparation and future directions. This slice has only been validated in juvenile animals. As is typical in the connected slice literature, the focus of these studies has been on young animals because of their resistance to slicing trauma and ease of visualization of neurons for patch recordings. It is recognized that many of the relevant cell types found in this slice undergo significant maturational changes during the first weeks of postnatal development (Kotak et al. 2008; Llano and Sherman 2009; Romand et al. 2011; Venkataraman and Bartlett 2013; Zhu et al. 2000). We have not yet systematically explored developmental changes in this slice preparation, although it is worth noting that this preparation may prove useful for probing developmental changes in colliculothalamocortical transmission.

Another potential limitation in this preparation is slice-to-slice variability in connectivity among IC, MGB, and AC. This is a problem with all connected slice preparations, but the problem may be compounded by the additional pathways that are contained in the currently described preparation. However, within a given slice, it is very easy to determine quickly what structures are connected using either flavoprotein or NAD imaging. In our experience, within 15 min of the slice being placed in the chamber, the experimenter can know the degree of connectivity that exists in that slice. Once baseline connectivity is established, various manipulations can be performed, and comparisons can be made relative to baseline conditions.

Although there are other approaches to the study of long-range pathway in brain slices, such as the use of viral-mediated transfer of optogenetic probes, which label axons and may permit the cutting of more simple brain slices (Petreanu et al. 2007), such approaches may not easily allow the study of multiple brain regions or the integration of multiple inputs on a single brain region simultaneously. It is worth noting that it may be possible to combine the current IC-MGB-AC slice with other techniques to allow the study of the impact of longer-range projections on auditory thalamocortical transmission. For example, the combination of this slice with optogenetic approaches can be used to investigate the impact of spatially remote structures, such as the prefrontal cortex, amygdala, and brain stem, on the transmission of information through the midbrain-thalamocortical pathway. Therefore, this slice preparation, on its own or when combined with other modern approaches, may open up avenues of investigation not previously available to scientists working in either the auditory forebrain or the thalamocortical systems more broadly.

DISCLOSURES

No conflicts of interest, financial or otherwise, are declared by the author(s).

AUTHOR CONTRIBUTIONS

D.A.L. and B.J.S. conception and design of research; D.A.L., B.J.S., A.M.H.L., and K.A.S. performed experiments; D.A.L., B.J.S., and A.M.H.L. analyzed data; D.A.L. interpreted results of experiments; D.A.L. prepared figures; D.A.L. drafted manuscript; D.A.L. and B.J.S. edited and revised manuscript; D.A.L., B.J.S., A.M.H.L., and K.A.S. approved final version of manuscript.

REFERENCES

Agmon A, Connors BW. Correlation between intrinsic firing patterns and thalamocortical synaptic responses of neurons in mouse barrel cortex. *J Neurosci* 12: 319–329, 1992.

Agmon A, Connors BW. Thalamocortical responses of mouse somatosensory (barrel) cortex in vitro. *Neuroscience* 41: 365–379, 1991.

Aitken P, Breese G, Dudek F, Edwards F, Espanol M, Larkman P, Lipton P, Newman G, Nowak T, Panizzon K. Preparative methods for brain slices: a discussion. *J Neurosci Res* 59: 139–149, 1995.

Bajo VM, Moore DR. Descending projections from the auditory cortex to the inferior colliculus in the gerbil, *Meriones unguiculatus*. *J Comp Neurol* 486: 101–116, 2005.

Bajo VM, Nodal FR, Bizley JK, Moore DR, King AJ. The ferret auditory cortex: descending projections to the inferior colliculus. *Cereb Cortex* 17: 475–491, 2007.

Bajo VM, Nodal FR, Moore DR, King AJ. The descending corticocollicular pathway mediates learning-induced auditory plasticity. *Nat Neurosci* 13: 253–260, 2010.

Bartlett EL, Smith PH. Anatomic, intrinsic, and synaptic properties of dorsal and ventral division neurons in rat medial geniculate body. *J Neurophysiol* 81: 1999–2016, 1999.

Bartlett EL, Wang X. Neural representations of temporally modulated signals in the auditory thalamus of awake primates. *J Neurophysiol* 97: 1005–1017, 2007.

Beyerl BD. Afferent projections to the central nucleus of the inferior colliculus in the rat. *Brain Res* 145: 209–223, 1978.

Budinger E, Heil P, Scheich H. Functional organization of auditory cortex in the Mongolian gerbil (*Meriones unguiculatus*). III. Anatomical subdivisions and corticocortical connections. *Eur J Neurosci* 12: 2425–2451, 2000.

Castro-Alamancos MA, Calcagnotto ME. Presynaptic long-term potentiation in corticothalamic synapses. *J Neurosci* 19: 9090–9097, 1999.

Cruikshank SJ, Killackey HP, Metherate R. Parvalbumin and calbindin are differentially distributed within primary and secondary subregions of the mouse auditory forebrain. *Neuroscience* 105: 553–569, 2001.

Cruikshank SJ, Rose HJ, Metherate R. Auditory thalamocortical synaptic transmission in vitro. *J Neurophysiol* 87: 361–384, 2002.

Faye-Lund H, Osen KK. Anatomy of the inferior colliculus in rat. *Anat Embryol (Berl)* 171: 1–20, 1985.

Feng AS, Lin W. Differential innervation patterns of three divisions of frog auditory midbrain (torus semicircularis). *J Comp Neurol* 306: 613–630, 2004.

Finlayson P, Cynader M. Synaptic depression in visual cortex tissue slices: an in vitro model for cortical neuron adaptation. *Exp Brain Res* 106: 145–155, 1995.

Gil Z, Connors BW, Amitai Y. Efficacy of thalamocortical and intracortical synaptic connections: quanta, innervation, and reliability. *Neuron* 23: 385–397, 1999.

Hackett TA, Barkat TR, O'Brien BM, Hensch TK, Polley DB. Linking topography to tonotopy in the mouse auditory thalamocortical circuit. *J Neurosci* 31: 2983–2995, 2011.

Hashikawa T, Rausell E, Molinari M, Jones EG. Parvalbumin- and calbindin-containing neurons in the monkey medial geniculate complex: differential distribution and cortical layer specific projections. *Brain Res* 544: 335–341, 1991.

Hatfield R, Mendelow A, Perry R, Alvarezs L, Modha P. Triphenyltetrazolium chloride (TTC) as a marker for ischaemic changes in rat brain following permanent middle cerebral artery occlusion. *Neuropathol Appl Neurobiol* 17: 61–67, 1991.

Holy TE, Guo Z. Ultrasonic songs of male mice. *PLoS Biol* 3: e386, 2005.

Husson TR, Issa NP. Functional imaging with mitochondrial flavoprotein autofluorescence: theory, practice, and applications. In: *In Vivo Optical Imaging of Brain Function* (2nd ed.), edited by Frostig RD. Boca Raton, FL: CRC Press, 2009, chapt. 8.

Husson TR, Mallik AK, Zhang JX, Issa NP. Functional imaging of primary visual cortex using flavoprotein autofluorescence. *J Neurosci* 27: 8665–8675, 2007.

Jen P, Sun X, Chen Q. An electrophysiological study of neural pathways for corticofugally inhibited neurons in the central nucleus of the inferior colliculus of the big brown bat, *Eptesicus fuscus*. *Exp Brain Res* 137: 292–302, 2001.

Jones EG. The thalamic matrix and thalamocortical synchrony. *Trends Neurosci* 24: 595–601, 2001.

Katz LC, Dalva MB. Scanning laser photostimulation: a new approach for analyzing brain circuits. *J Neurosci Methods* 54: 205–218, 1994.

Kawaguchi Y, Wilson CJ, Emson PC. Intracellular recording of identified neostriatal patch and matrix spiny cells in a slice preparation preserving cortical inputs. *J Neurophysiol* 62: 1052–1068, 1989.

Kosterin P, Kim G, Muschol M, Obaid A, Salzberg B. Changes in FAD and NADH fluorescence in neurosecretory terminals are triggered by calcium entry and by ADP production. *J Membr Biol* 208: 113–124, 2005.

Kotak VC, Takesian AE, Sanes DH. Hearing loss prevents the maturation of GABAergic transmission in the auditory cortex. *Cereb Cortex* 18: 2098–2108, 2008.

Kubota Y, Kamatani D, Tsukano H, Ohshima S, Takahashi K, Hishida R, Kudoh M, Takahashi S, Shibuki K. Transcranial photo-inactivation of neural activities in the mouse auditory cortex. *Neurosci Res* 60: 422–430, 2008.

Kuwabara N. Neuroanatomic technique for studying long axonal projections in the central nervous system: combined axonal staining and pre-labeling in parasagittal gerbil brain slices. *Biotech Histochem* 87: 413–422, 2012.

Kuwabara N, Zook JM. Geniculo-collicular descending projections in the gerbil. *Brain Res* 878: 79–87, 2000.

Langner G. Periodicity coding in the auditory system. *Hear Res* 60: 115–142, 1992.

Lee CC, Sherman SM. Topography and physiology of ascending streams in the auditory tectothalamic pathway. *Proc Natl Acad Sci USA* 107: 372–377, 2010.

Lee CM, Chang WC, Chang KB, Shyu BC. Synaptic organization and input-specific short-term plasticity in anterior cingulate cortical neurons with intact thalamic inputs. *Eur J Neurosci* 25: 2847–2861, 2007.

Li Y, Evans MS, Faingold CL. Synaptic response patterns of neurons in the cortex of rat inferior colliculus. *Hear Res* 137: 15–28, 1999.

Liu R, Miller K, Merzenich M, Schreiner C. Acoustic variability and distinguishability among mouse ultrasound vocalizations. *J Acoust Soc Am* 114: 3412–3422, 2003.

Llano DA, Feng AS. Response characteristics of neurons in the medial geniculate body of the little brown bat to simple and temporally-patterned sounds. *J Comp Physiol A* 184: 371–385, 1999.

Llano DA, Sherman SM. Differences in intrinsic properties and local network connectivity of identified layer 5 and layer 6 adult mouse auditory cortico-thalamic neurons support a dual corticothalamic projection hypothesis. *Cereb Cortex* 19: 2810–2826, 2009.

Llano DA, Sherman SM. Evidence for nonreciprocal organization of the mouse auditory thalamocortical-corticothalamic projection systems. *J Comp Neurol* 507: 1209–1227, 2008.

Llano DA, Theyel BB, Mallik AK, Sherman SM, Issa NP. Rapid and sensitive mapping of long-range connections in vitro using flavoprotein autofluorescence imaging combined with laser photostimulation. *J Neurophysiol* 101: 3325–3340, 2009.

Llinas RR, Leznik E, Urbano FJ. Temporal binding via cortical coincidence detection of specific and nonspecific thalamocortical inputs: a voltage-dependent dye-imaging study in mouse brain slices. *Proc Natl Acad Sci USA* 99: 449–454, 2002.

MacLean JN, Fenstermaker V, Watson BO, Yuste R. A visual thalamo-cortical slice. *Nat Methods* 3: 129–134, 2006.

Malmierca MS, Ryugo DK. Descending connections of auditory cortex to the midbrain and brain stem. In: *The Auditory Cortex*, edited by Winer JA and Schreiner CE. New York: Springer, 2011, p. 189–208.

Mathews KS, McLaughlin DP, Ziabari LH, Toner CC, Street PC, Hisgrove E, Bezzina EL, Stamford JA. Rapid quantification of ischaemic injury and cerebroprotection in brain slices using densitometric assessment of 2, 3, 5-triphenyltetrazolium chloride staining. *J Neurosci Methods* 102: 43–51, 2000.

Meininger V, Pol D, Derer P. The inferior colliculus of the mouse. A Nissl and Golgi study. *Neuroscience* 17: 1159–1179, 1986.

Miles R, Wong R. Inhibitory control of local excitatory circuits in the guinea-pig hippocampus. *J Physiol* 388: 611–629, 1987.

Mitani A, Shimokouchi M, Nomura S. Effects of stimulation of the primary auditory cortex upon colliculogeniculate neurons in the inferior colliculus of the cat. *Neurosci Lett* 42: 185–189, 1983.

Peruzzi D, Bartlett E, Smith PH, Oliver DL. A monosynaptic GABAergic input from the inferior colliculus to the medial geniculate body in rat. *J Neurosci* 17: 3766–3777, 1997.

Petreanu L, Huber D, Sobczyk A, Svoboda K. Channelrhodopsin-2-assisted circuit mapping of long-range callosal projections. *Nat Neurosci* 10: 663–668, 2007.

Reichova I, Sherman SM. Somatosensory corticothalamic projections: distinguishing drivers from modulators. *J Neurophysiol* 92: 2185–2197, 2004.

Reinert KC, Gao W, Chen G, Ebner TJ. Flavoprotein autofluorescence imaging in the cerebellar cortex in vivo. *J Neurosci Res* 85: 3221–3232, 2007.

Richardson RJ, Blundon JA, Bayazitov IT, Zakharenko SS. Connectivity patterns revealed by mapping of active inputs on dendrites of thalamorecipient neurons in the auditory cortex. *J Neurosci* 29: 6406–6417, 2009.

Richerson GB, Messer C. Effect of composition of experimental solutions on neuronal survival during rat brain slicing. *Exp Neurol* 131: 133–143, 1995.

Romand S, Wang Y, Toledo-Rodriguez M, Markram H. Morphological development of thick-tufted layer V pyramidal cells in the rat somatosensory cortex. *Front Neuroanat* 5: 5, 2011.

Saldaña E, Feliciano M, Mugnaini E. Distribution of descending projections from primary auditory neocortex to inferior colliculus mimics the topography of intracollicular projections. *J Comp Neurol* 371: 15–40, 1996.

Schofield BR. Projections to the inferior colliculus from layer VI cells of auditory cortex. *Neuroscience* 159: 246–258, 2009.

Senatorov VV, Hu B. Extracortical descending projections to the rat inferior colliculus. *Neuroscience* 115: 243–250, 2002.

Shepherd GM, Pologruto TA, Svoboda K. Circuit analysis of experience-dependent plasticity in the developing rat barrel cortex. *Neuron* 38: 277–289, 2003.

Sherman SM, Guillery RW. Distinct functions for direct and transthalamic corticocortical connections. *J Neurophysiol* 106: 1068–1077, 2011.

Shibuki K, Hishida R, Murakami H, Kudoh M, Kawaguchi T, Watanabe M, Watanabe S, Kouuchi T, Tanaka R. Dynamic imaging of somatosensory cortical activity in the rat visualized by flavoprotein autofluorescence. *J Physiol* 549: 919–927, 2003.

Shuttleworth CW, Brennan AM, Connor JA. NAD (P) H fluorescence imaging of postsynaptic neuronal activation in murine hippocampal slices. *J Neurosci* 23: 3196–3208, 2003.

Slater BJ, Willis AM, Llano DA. Evidence for layer-specific differences in auditory corticocollicular neurons. *Neuroscience* 229: 144–154, 2013.

Smith JC, Ellenberger HH, Ballanyi K, Richter DW, Feldman JL. Pre-Bötzinger complex: a brainstem region that may generate respiratory rhythm in mammals. *Science* 254: 726–729, 1991.

Smith PH, Bartlett EL, Kowalkowski A. Cortical and collicular inputs to cells in the rat paralaminar thalamic nuclei adjacent to the medial geniculate body. *J Neurophysiol* 98: 681–695, 2007.

Spergel DJ, Krüth U, Shimshek DR, Sprengel R, Seeburg PH. Using reporter genes to label selected neuronal populations in transgenic mice for gene promoter, anatomical, and physiological studies. *Prog Neurobiol* 63: 673–686, 2001.

Suga N, Ma X. Multiparametric corticofugal modulation and plasticity in the auditory system. *Nat Rev Neurosci* 4: 783–794, 2003.

Ter-Mikaelian M, Sanes DH, Semple MN. Transformation of temporal properties between auditory midbrain and cortex in the awake mongolian gerbil. *J Neurosci* 27: 6091–6102, 2007.

Theyel BB, Llano DA, Sherman SM. The corticothalamocortical circuit drives higher-order cortex in the mouse. *Nat Neurosci* 13: 84–88, 2010.

Venkataraman Y, Bartlett EL. Postnatal development of synaptic properties of the GABAergic projection from the inferior colliculus to the auditory thalamus. *J Neurophysiol* 109: 2866–2882, 2013.

Verbny YI, Erdélyi F, Szabó G, Banks MI. Properties of a population of GABAergic cells in murine auditory cortex weakly excited by thalamic stimulation. *J Neurophysiol* 96: 3194–3208, 2006.

Wallace MN, Kitzes LM, Jones EG. Chemoarchitectonic organization of the cat primary auditory cortex. *Exp Brain Res* 86: 518–526, 1991.

Winer JA, Chernock ML, Larue DT, Cheung SW. Descending projections to the inferior colliculus from the posterior thalamus and the auditory cortex in rat, cat, and monkey. *Hear Res* 168: 181–195, 2002.

Yan J, Ehret G. Corticofugal modulation of midbrain sound processing in the house mouse. *Eur J Neurosci* 16: 119–128, 2002.

Yan J, Zhang Y, Ehret G. Corticofugal shaping of frequency tuning curves in the central nucleus of the inferior colliculus of mice. *J Neurophysiol* 93: 71–83, 2005.

Zhu JJ, Esteban JA, Hayashi Y, Malinow R. Postnatal synaptic potentiation: delivery of GluR4-containing AMPA receptors by spontaneous activity. *Nat Neurosci* 3: 1098–1106, 2000.